THE EFFECT OF DEFORMATION ON GRAIN BOUNDARY WETNESS IN PARTIALLY MOLTEN PERIDOTITE

A Senior Scholars Thesis

by

STEPHEN E. SCHNEIDER

Submitted to the Office of Undergraduate Research
Texas A&M University
in partial fulfillment of the requirements for the designation as

UNDERGRADUATE RESEARCH SCHOLAR

April 2006

Major: Geophysics

THE EFFECT OF DEFORMATION ON GRAIN BOUNDARY WETNESS IN PARTIALLY MOLTEN PERIDOTITE

A Senior Scholars Thesis

by

STEPHEN E. SCHNEIDER

Submitted to the Office of Undergraduate Research
Texas A&M University
in partial fulfillment of the requirements for the designation as

UNDERGRADUATE RESEARCH SCHOLAR

Approved by:

Research Advisor:	David W. Sparks
Associate Dean for Undergraduate Research:	Robert C. Webb

April 2006

Major: Geophysics

ABSTRACT

The Effect of Deformation on Grain Boundary Wetness in Partially Molten Peridotite
(April 2006)

Stephen E. Schneider
Department of Geology and Geophysics
Texas A&M University

Research Advisor: Dr. David W. Sparks
Department of Geology and Geophysics

The spatial distribution of the melt phase can affect many properties of partially molten rocks, including viscosity and seismic wave velocity. A good way to quantify this distribution is the grain boundary wetness, the fraction of total grain boundaries that are in contact with melt. This goal of this study was to quantify the effect of deformation on grain boundary wetness. We analyzed three prepared samples consisting of olivine and 3%, 7% or 15% of a basalt melt phase, which were equilibrated at 1250˚C, 300 MPa of confining stress and <50 MPa of differential stress. We describe a process developed to calculate the grain boundary wetness from prepared SEM images of the samples. We find an expected dependence of wetness on porosity. The effect of deformation was not consistent across all three samples: the two higher melt fraction samples show greater wetness before deformation, while the 3% melt sample showed no effect. This result

does not agree with experiments on an organic analog material, which indicated that deformation increases wetness. If viscosity increases with wetness, the results of this study indicate that partially molten peridotite strengthen with deformation, which would have important implications for mantle dynamics. Some researchers have proposed that if you deform a sample of partially molten peridotite it will in fact raise the grain boundary wetness Takei [private communication, 2004]. This statement is bold because if you raise the wetness of the sample then the viscosity goes down thereby making the specimen weaker. Our results show that deformation does not have a consistent discernible effect on grain boundary wetness in partially molten peridotite.

TABLE OF CONTENTS

Page

ABSTRACT iii

TABLE OF CONTENTS v

LIST OF FIGURES vi

1. INTRODUCTION: THE IMPORTANCE OF GRAIN BOUNDARY WETNESS 1

2. METHODOLOGY 7

2.1 Preparation of partially-molten samples 7
2.2 Imaging melt and grain boundaries 9

3. RESULTS AND ANALYSIS 12

4. DISCUSSION AND CONCLUSIONS 26

REFERENCES 28

CONTACT INFORMATION 30

LIST OF FIGURES

FIGURE Page

1 An idealized graphical representation of a partially-molten material, with melt confined to the points where three grains come together (triple junctions).. 4

2 Actual SEM micrograph of sample PI-1108_01 taken at the Characterization Facility with a Jeol 6500. 5

3 Binary image created from an SEM image of sample PI_1108_01 (see Figure 2) to obtain the area of the solid-liquid boundaries. 11

4 Image of solid-solid grain boundaries traced from SEM image PI_1108_01. 11

5 Shown in this figure is a plot of ψ vs. ϕ and two enveloping curves of $\psi=B\phi^{1/2}$ represented by the green and red curves with B values of 1.7 and 2.3. 14

6 Wetness vs. melt fraction for the 3% MORB samples. 17

7 Wetness vs. melt fraction for the 7% MORB samples. 18

8 Wetness vs. melt fraction for the 15% MORB samples. 19

9 The area of the solid-solid grain contact vs. melt fraction for all images, and a linear fit to this data. 21

10 The area of the solid-liquid grain boundaries vs. melt fraction.....22

11 A_{sl} vs. A_{ss}, and the best fit line. 24

12 Same data shown in Figure 11., with different symbols used for the different samples. 25

1. INTRODUCTION: THE IMPORTANCE OF GRAIN BOUNDARY WETNESS

Regions of partially-molten peridotite underlie many geologically important regions, such as oceanic spreading centers, rift zones, subduction arcs, and intraplate hotspots, and have been proposed to exist in deeper regions of the mantle (e.g., Revenaugh and Sipkin, 1994). The detectability of this partial melt and its effect on mantle dynamics depends on the both the amount of melt, and how it is distributed within the crystalline matrix. The distribution of the liquid phase is crucial to understanding the elasticity, viscosity, and permeability of a partially molten rock [Bulau et al., 1979; von Bargen and Waff, 1986; Watson and Brenan, 1987].

The equilibrium distribution of a melt phase among grains is determined by the surface energies on the grain boundaries. For an ideal system of isotropic grains, the distribution can be theoretically calculated as a function of these energies [Waff and Bulau, 1979; von Bargen and Waff, 1986]. The ratio of the solid-liquid and solid-solid interfacial energies determines the dihedral angle, the angle made at the intersection of a solid-solid boundary with a pore [Kohlstedt and Cooper, 1986]. When this angle is less than 60˚, as is the case for an olivine/basaltic melt system, the melt will be distributed in a network of interconnected tubes. If the dihedral angle is greater than 60˚, small amounts of melt will form isolated pores [Watson et al., 1982].

This thesis follows the style of *Journal of Geophysical Research.*

Researchers have postulated that partially molten peridotite should be different from the ideal model, though. Most silicate minerals are not isotropic, i.e., the surface energies vary with crystallographic orientation. Therefore the ideal model is complicated by “faceting” of grain faces which causes melt to be distributed in thinner sheets along more of the grain boundaries [e.g., Waff and Faul, 1992]. Actual pore geometries in laboratory models of partially-molten upper mantle show a wide variety of pore sizes and shapes (see Figure. 2). The evolution of pore geometries under various mechanical conditions is also poorly understood. Some researchers have proposed that the deformation of partially molten peridotite will also change the distribution of melt [Faul, 1992; Takei, in prep., 2005].

As a result, a more empirical measure of the distribution has been used: the grain boundary wetness [Takei, in prep., 2005]. Wetness is defined as the ratio of solid-liquid boundary area to the total area of interphase boundaries, i.e., the fraction of total grain boundaries that are wet. The complement to wetness, the contiguity, is 1 minus the wetness. Contiguity has been shown to be related to the velocity of seismic waves in a medium [Takei, 1998].

Grain boundary wetness ψ is defined in the model of Takei (1998) as

$$\psi = \frac{A_{sl}}{A_{sl} + 2A_{ss}} \qquad (1)$$

where A_{sl} is the interfacial area of the solid-liquid grain boundary (see Figure. 1). A_{ss} is the interfacial area of the solid-solid grain boundary. Extensive testing by Yoshino et al., [2005] argues that the most accurate method to quantify the textural equilibrium of a rock is to measure its grain boundary wetness. The definition of wetness is applied to two-dimensional cross-sectional images of partially molten rock by redefining the interfacial areas as interfacial lengths [Yoshino et al., 2005].

The grain boundary wetness of a sample could depend on the melt fraction, and the size and shape of the grains and pores. A greater melt fraction will increase the area of the solid-melt boundary, therby raising the grain boundary wetness according to Eqn. 1. Theoretical (Waff and Bulau et al., 1979) and experimental (Yoshino et al., 2005) studies predict that wetness increases with the square root of melt fraction.

Variations in the value of wetness at a given melt fraction must be due to a changing distribution of the melt phase. A relatively high value of wetness would result if the melt is distributed in narrow films along grain boundaries. This sort of distribution could decrease the viscosity of the rock, and the velocity of seismic waves, while decreasing the permeability.

In textural equilibrium, contiguity is uniquely determined as a function of melt fraction and dihedral angle [e.g., von Bargen and Waff, 1986; Takei, 2002]. However, Jin et al., [1994] and Bai et al., [1997] reported that the grain boundaries were significantly wetted by melt in deformed partially molten peridotites. These results show that grain boundary wetness is a variable that evolves independently from the melt fraction. In contrast, dynamic wetting did not occur in experimental study of Hirth and

Kohlstedt [1995a,b] performed under similar conditions to Jin et al., [1995] and Bai et al., [1997].

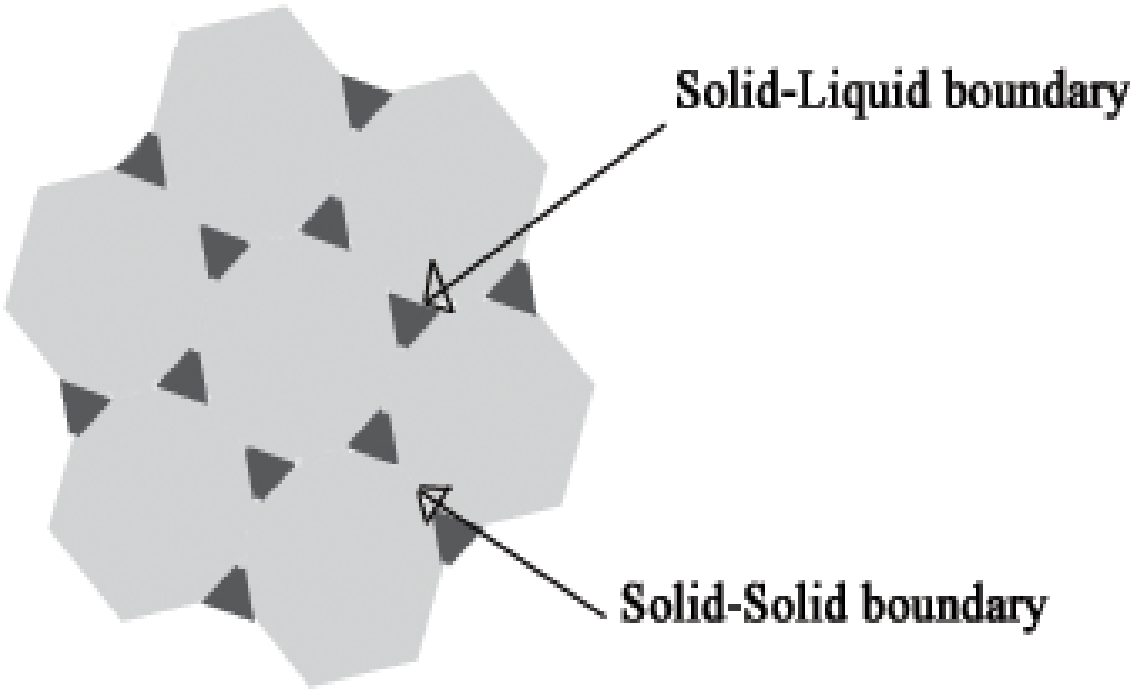

Figure 1. An idealized graphical representation of a partially-molten material, with melt confined to the points where three grains come together (triple junctions). The solid-solid grain boundaries and the solid-liquid grain boundaries are used for the calculation of grain boundary wetness.

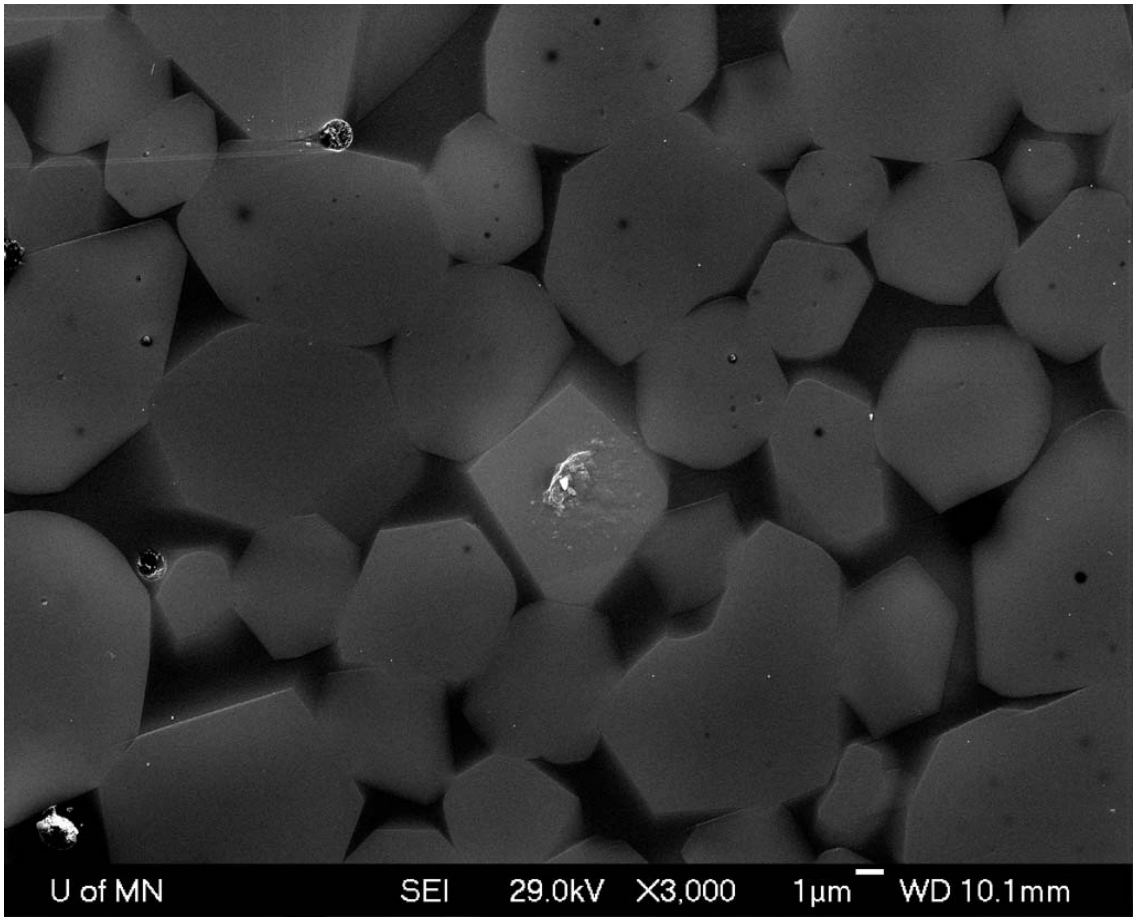

Figure 2. Actual SEM micrograph of sample PI-1108_01 taken at the Characterization Facility with a Jeol 6500. This image shows a great contrast difference between grains and melt. Image was taken at 29kV and a relative current of 13.

Takei et al., [2005] studied the effect of deformation on a partially molten organic system consisting of crystalline borneol and diphenylamine, which melts at 60˚C. This system is an analog to partially molten peridotite, because the borneol undgoes ductile deformation in a similar manner to silicates, and the dihedral angle is similar to that for olivine and basaltic melt. Takei discovered dynamic wetting while deforming the analog material. They found a consistent enhancement of grain boundary wetting in deformed samples.

In this project, we take a systematic approach to analyzing SEM images to better understand what happens to a specimen's grain boundary wetness after a differential stress between 5 and 50 MPa is applied to it. We present a methodology for creating and analyzing the grain boundary wetness of partially molten rocks. Several samples were examined with different fractions of solid (olivine) and melt (basalt), formed under both hydrostatic and differential stress conditions. SEM images were processed to calculate the porosity and wetness for each image. The results show expected trends of wetness with melt fraction, and some indication that, at least at melt fractions > 5%, deformed samples had a lower grain boundary wetness. There is however, significant variation between samples.

2. METHODOLOGY

2.1 Preparation of partially-molten samples

The first step in calculating grain boundary wetness ψ was to prepare the synthetic samples of peridotite. Samples PI-19, GH-92, 1108, and 1107 were previously synthesized by Hirth and Kohlstedt (1995) prior to the start of the experiment, while samples 1241 deformed and undeformed were created for this study. Samples were made from powdered San Carlos olivine (~Fo_{91}) crystals to represent peridotite and powdered Mid-ocean Ridge Basalt (MORB) to represent the melt phase. The MORB is an olivine tholeiite, which was previously used in other experimental studies on partially molten rocks [e.g. Riley and Kohlstedt, 1991; Daines and Kohlstedt, 1993]. The olivine was crushed into powder in a mortar bowl to achieve average grain sizes between 10 to 25 μm, and the MORB had particle sizes less than 8 μm (Daines and Kohlstedt 1993). The MORB was mechanically mixed with olivine powder. Each sample was fabricated under dry conditions and cold pressed into Ni cans. Because grain boundary wetness increases with melt fraction, we analyzed three samples made with 3, 7 and 15 wt% MORB. The samples were hot pressed at 300MPa and a temperature of 1250^{o}C for 4 hours in a Paterson Apparatus, which is a servo-controlled internally heated gas-medium that uses Argon as a confining medium. The MORB powder melts to form the melt phase during this stage. The temperature during the experiments was both controlled and monitored using a chromel-alumel thermocouple. Nickel jackets and sleeves were used in all experiments to buffer the oxygen fugacity.

Each hot-pressed sample was quenched and divided. One part of the sample was deformed in uniaxial compression. That sample was returned to the Paterson Apparatus and brought back to 300MPa and 1250^{o}C, and a differential stress between 5 and 50 MPa for 4 hours.

Both undeformed and deformed samples were cut perpendicular and parallel to their long axes. Both of the cut surfaces were imaged. Polishing the sample for scanning electron microscopy proved to be challenging. After much trial and error, polishing of the samples was most effective with 30 μm, 15 μm, 6 μm, 3 μm, and finally 0.01 μm diamond lapping film until there was a shiny reflective surface. The reflective surface was indicative of a smooth scanning surface with some topography due to melt. Topography of the surface was essential because it allowed for optimal image acquisition with the scanning electron microprobe. Imaging of the polished samples of peridotite was performed with a Jeol-6500 SEM at the University of Minnesota's Characterization Facility. The size of each image ranged from 640 x 480 to 2561 x 1934 pixels. Figure 2 shows an SEM with a clear contrast between the melt and the and well defined grain boundaries. This high definition was necessary for the image analysis.

2.2 Imaging melt and grain boundaries

To calculate A_{sl}, the SEM images were processed using Photoshop to enhance the distinction between melt and solid. The contrast of the images was raised to create a binary image, in which solid grains were white and melt was black. For each image we used despeckle, dithering, auto-contrast, and threshold functions in Adobe Photoshop. The despeckle function removed any 1-5 pixel aggregates, which were not melt pockets. Any remaining stray pixels that were interpreted as "noise" were manually edited. Dithering was used to smooth the image, which allowed for a more accurate transition to a binary image. Auto-contrast was used to automatically adjust highlights and shadows to fix poor image contrast due to current fluctuations while imaging with the SEM. The threshold function converted the image from RGB to binary. We used a relative value of 24 with this threshold function to make sure each image was edited equally. The binary image resulting from the processing of Figure 2 is shown in Figure 3.

In a bitmap of these binary images, any black pixel that is bordered by a white pixel is considered to be solid-liquid boundary. We wrote a MATLAB script to distinguish and count the total number of boundary pixels. This number divided by the total number of pixels in the image gives the length of melt pocket perimeter per area of image, A_{sl}. Melt pocket perimeter A_{sl} was determined to be the length of the boundary around the melt pocket excluding any internal holes (see Figure. 2). The errors associated with perimeter measurements using this method are dependent on the size,

shape and orientation of the melt pocket analyzed and may be as large as 7% (Daines and Kohlstedt et al., 1997).

These binary images were also used to determine the melt fraction in each image, which can vary significantly from the melt fraction of the overall sample. MATLAB's processing tools were used to find the percentage of black (melt) pixels in an image. The melt fraction measured here is an area fraction, which we would expect to be slightly larger than the corresponding weight fraction, due to the density difference between MORB and olivine.

A different technique was used in the calculation of A_{ss}. The grain boundaries in the original SEM images were traced using Photoshop's "line tool" with one pixel wide lines. Each image was traced at 300x zoom to get precise representation of the grain boundaries. We also used Photoshop to adjust the opacity of the original SEM image to between 10% and 20%. This opacity was just enough to clearly see the solid/solid grain contacts without completely distorting the original SEM image. Figure 4 shows the traced grain boundaries superimposed on the original SEM image. The total number of solid/solid boundary pixels was counted using MATLAB's image processes tools. This number divided by the total number of pixels in the image gives the length of solid/solid grain boundaries per area of image, A_{ss}.

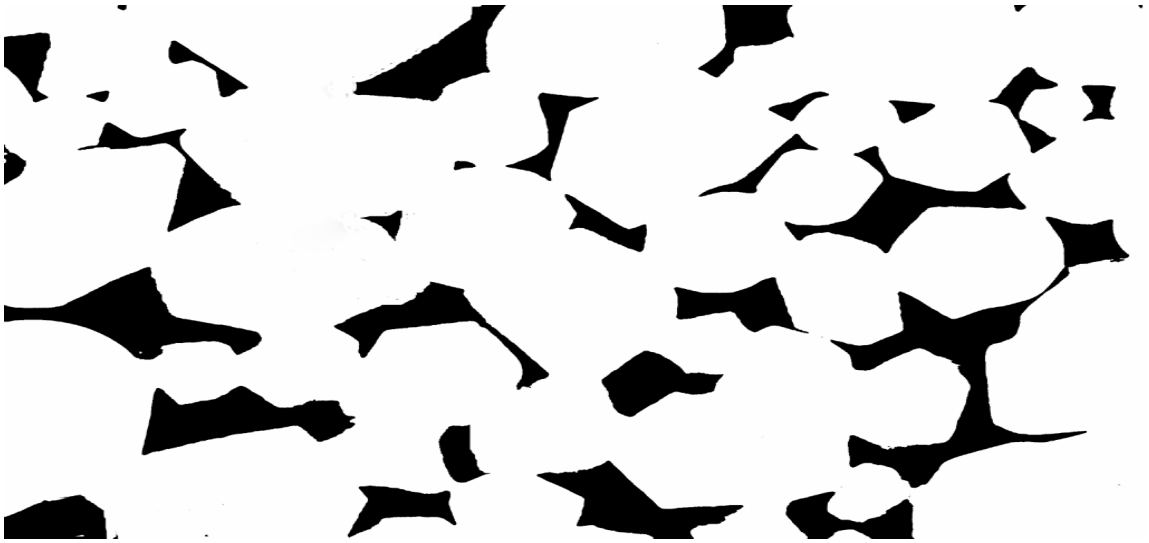

Figure 3. Binary image created from an SEM image of sample PI_1108_01 (see Figure 2) to obtain the area of the solid-liquid boundaries. Black represents melt and white represents grains.

Figure 4. Image of solid-solid grain boundaries traced from SEM image PI_1108_01 (see Figure 2). Each line was drawn to be approximately 1 pixel in width for greatest accuracy. Note that some lines don't exactly match with their corresponding melt pockets, because of a shadowing effect.

3. RESULTS AND ANALYSIS

This study examined three initial samples, created with 3%, 7% or 15% MORB component. Each original sample was divided into a pair of samples, one of which was then deformed while the other was left undeformed. Several SEM images were prepared for each sample, but some did not yeild samples that were clear enough to accurately determine A_{ss} and A_{sl}. The rest of this study will focus on the images for which grain boundary wetness could be determined: 3 images each for the deformed and undeformed samples with 3% MORB (1241 def and 1241 undef.); 7 images of the deformed sample (PI-19) and 10 images of the undeformed sample (GH92) with 7% MORB; 7 images of the deformed sample (1108) and 6 images of the undeformed sample (1107) with 15% MORB.

Each SEM image of a particular sample, because it contains a relatively small number of grains and pores, can have a melt fraction that varies significantly from the percentage of MORB in the original sample. The range of observed melt fractions ϕ was 0.03 to 0.08 in the 6 images of the 3% MORB samples, 0.05 to 0.21 in the 17 images of the 7% MORB sample, and 0.06 to 0.16 in the 13 images of the 15% MORB sample. Raw and calculated data for each sample is shown in Table 1.

Figure 5 shows that grain boundary wetness increases directly with observed melt fraction in our images. We expect this relationship between ψ and ϕ because A_{sl} is highly dependent on melt fraction. One would expect the grain boundary wetness to

monotomically increase with melt fraction. This direct relationship was also found by another researcher studying undeformed upper mantle rocks [Takei et al., 2005]. Figure 5 also shows two curves of the following form,

$$\Psi = B\phi^{1/2} \qquad (2)$$

Yoshino proposed the above relationship between wetness and melt fraction, with the B values 1.7 and 2.3 obtained from fits to a similar olivine-basalt system and a partially molten KLB-1 peridotite, respectively. Our data lies between these 2 curves, indicating a generally similar melt fraction relationship for our experiments as well.

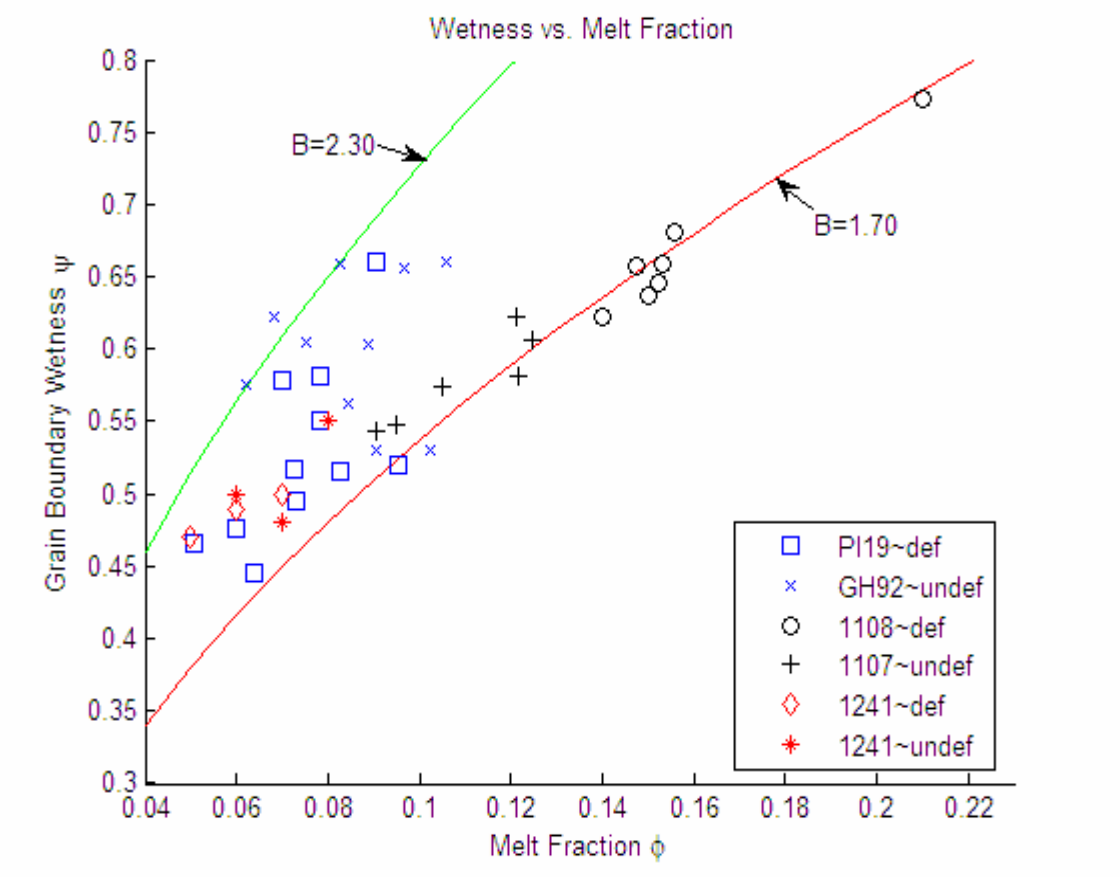

Figure 5. Shown in this figure is a plot of ψ vs. ϕ and two enveloping curves of $\psi=B\phi^{1/2}$ represented by the green and red curves with B values of 1.7 and 2.3.

Table 1. Shows the calcluated values for melt fraction, A_{sl}, GBW, and A_{ss}, Melt Fraction, normalized values of A_{ss} and A_{sl}, and values for B coeffs,. Samples in the set PI_19 and GH92-1 were made with a melt fraction on the order of 0.07, PI_1108 and PI_1107 were made with a melt fraction on the order of 0.15, and PI_1241 were made with a melt fraction on the order of 0.03

Sample	A_{ss}	A_{sl}	Melt Fraction	GBW	Norm A_{ss}	Norm A_{sl}	Image Resolution	B coeff
PI_19_05	12753	2.23E+04	0.0506	0.466	0.0026	0.0046	2561x1793	1.933
PI_19_07	10519	1.69E+04	0.0639	0.446	0.0021	0.0034	2561x1934	1.933
PI_19_08	9642	2.67E+04	0.0784	0.5808	0.0020	0.0055	2536x1928	1.933
PI_19_04	9338	2.55E+04	0.07	0.5778	0.0019	0.0052	2526x1929	1.933
1108_02	7116	4.87E+04	0.21	0.773	0.0015	0.0101	2561x1878	1.683
1108_03	3776	1.25E+04	0.14	0.6229	0.0031	0.0101	1280x966	1.683
1108_04	3664	1.28E+04	0.15	0.6363	0.0030	0.0104	1280x964	1.683
1108_05	6591	2.82E+04	0.156	0.6815	0.0013	0.0057	2560x198	1.683
1108_06	2575	9.41E+03	0.1525	0.6463	0.0033	0.0119	1024x770	1.683
1108_07	2604	9.98E+03	0.1476	0.657	0.0033	0.0126	1024x771	1.683
1108_01	1536	5.95E+03	0.153	0.659	0.0050	0.0193	640x481	1.683
1107_01	4460	1.24E+04	0.1218	0.5812	0.0056	0.0157	1024x771	1.737
1107_03	4504	10962	0.095	0.548	0.0057	0.0139	1024x771	1.737
1107_04	5103	1.38E+04	0.1049	0.5748	0.0065	0.0175	1024x771	1.737
1107_05	5146	1.22E+04	0.0907	0.5432	0.0065	0.0155	1024x770	1.737
1107_06	3541	1.09E+04	0.1249	0.6064	0.0045	0.0138	1024x771	1.737
1107_07	2680	7.16E+03	0.066	0.5747	0.0034	0.0091	1024x770	1.737
GH92-1	2449	6.61E+03	0.062	0.5755	0.0031	0.0084	1024x771	2.163
GH92-4	2892	8.76E+03	0.1023	0.53	0.0037	0.0111	1024x771	2.163
GH92-3	3183	9.69E+03	0.089	0.6034	0.0040	0.0123	1024x771	2.163
GH92-5	3504	9.00E+03	0.0843	0.5622	0.0044	0.0114	1024x771	2.163
GH92-6	2948	9.00E+03	0.0751	0.6042	0.0037	0.0114	1024x770	2.163
GH92-7	2749	9.07E+03	0.0681	0.6225	0.0035	0.0115	1024x771	2.163
GH92-8	3188	1.23E+04	0.0825	0.6589	0.0040	0.0156	1024x771	2.163
GH92-9	2471	9.41E+03	0.0969	0.6556	0.0031	0.0119	1024x771	2.163
GH92-10	6305	2.45E+04	0.106	0.6609	0.0013	0.0050	2560x1928	2.163
GH92-11	10328	2.31E+04	0.0906	0.53	0.0021	0.0047	2560x1928	2.163
PI_19_01	4289	9.74E+03	0.0954	0.52	0.0054	0.0123	1024x771	1.933
PI_19_02	6611	2.58E+04	0.0907	0.6609	0.0013	0.0052	2560x1928	1.933
PI_19_03	3391	6.16E+03	0.06	0.4759	0.0043	0.0078	1024x771	1.933
PI_19_09	4355	8.55E+03	0.073	0.4953	0.0055	0.0108	1024x771	1.933
PI_19_06	3157	7.61E+03	0.0783	0.55	0.0040	0.0096	1024x771	1.933
PI_19_10	3617	7.74E+03	0.0726	0.5169	0.0046	0.0098	1024x771	1.933
PI_19_11	4198	8.93E+03	0.0829	0.5155	0.0053	0.0113	1024x771	1.933
1241_DEF_1	7738	1.45E+04	0.0585	0.48	0.0016	0.0029	2560x1924	1.986
1241_UND_1	6170	1.66E+04	0.0836	0.55	0.0013	0.0034	2560x1928	1.941
1241_UND_2	10743	2.12E+04	0.06	0.4965	0.0022	0.0043	2560x1928	1.941
1241_DEF_2	6591	3.06E+04	0.17	0.7	0.0013	0.0062	2560x1924	1.986
1241_UND_3	6968	1.31E+04	0.0755	0.4838	0.0014	0.0026	2560x1928	1.941

Figures 6-8 show the melt fraction-wetness for each sample pair. For each sample, the data from usable images was fit with a curve of form (2). The best-fit value of the B parameter is given in Table 1. For the 3% MORB samples (Figure 6) the value for B was calculated to be 1.962 for the undeformed sample 1241 and 1.986 for the deformed sample of 1241. However, the data from these experiments don't fit the $\psi-\phi$ relationship very well, so the difference in B values is probably not meaningful. The different dependence on melt fraction could be indicating that the distribution of melt at low melt fractions is fundamentally different from that at higher melt fractions. Yoshino (2005), using a more powerful microscope, found that at extremely low melt fractions ($\phi<0.02$), most of the melt pockets occur in triple junctions, and grains are poorly wetted. He also observed that melt distributions are homogenous at $\phi<0.12$ and appear to be well wetted.

Both of the higher melt fraction experiments seem to indicate that the wetness is lower in the deformed sample, although the affect may not be significant at the higher melt fraction. In the 7% MORB sample (Figure 7) the value for B is 2.163 for the undeformed sample (GH92-1) and 1.933 for the deformed sample (PI19). Contrary to the 3% MORB sample, there is a considerably higher grain boundary wetness in the deformed sample. In the 15% MORB sample (Figure 8) the value for B is 1.737 for the undeformed sample 1107 and 1.683 for the deformed sample 1108. As with the 7% MORB samples, the undeformed sample has a slightly higher grain boundary wetness, however the effect is quite small.

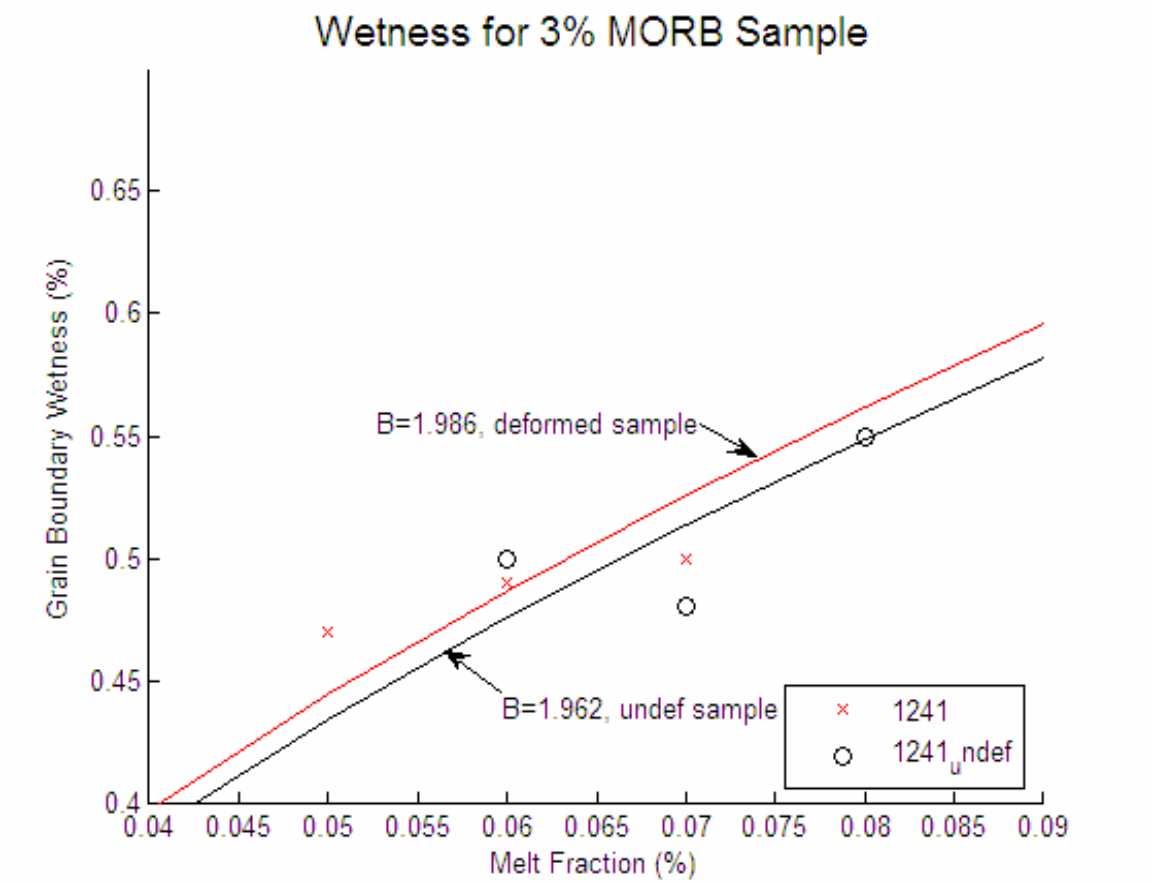

Figure 6. Wetness vs. melt fraction for the 3% MORB samples. The curves are fits of Eqn. 2, B values of 1.962 for the undeformed sample of 1241 and 1.986 for the deformed sample of 1241.

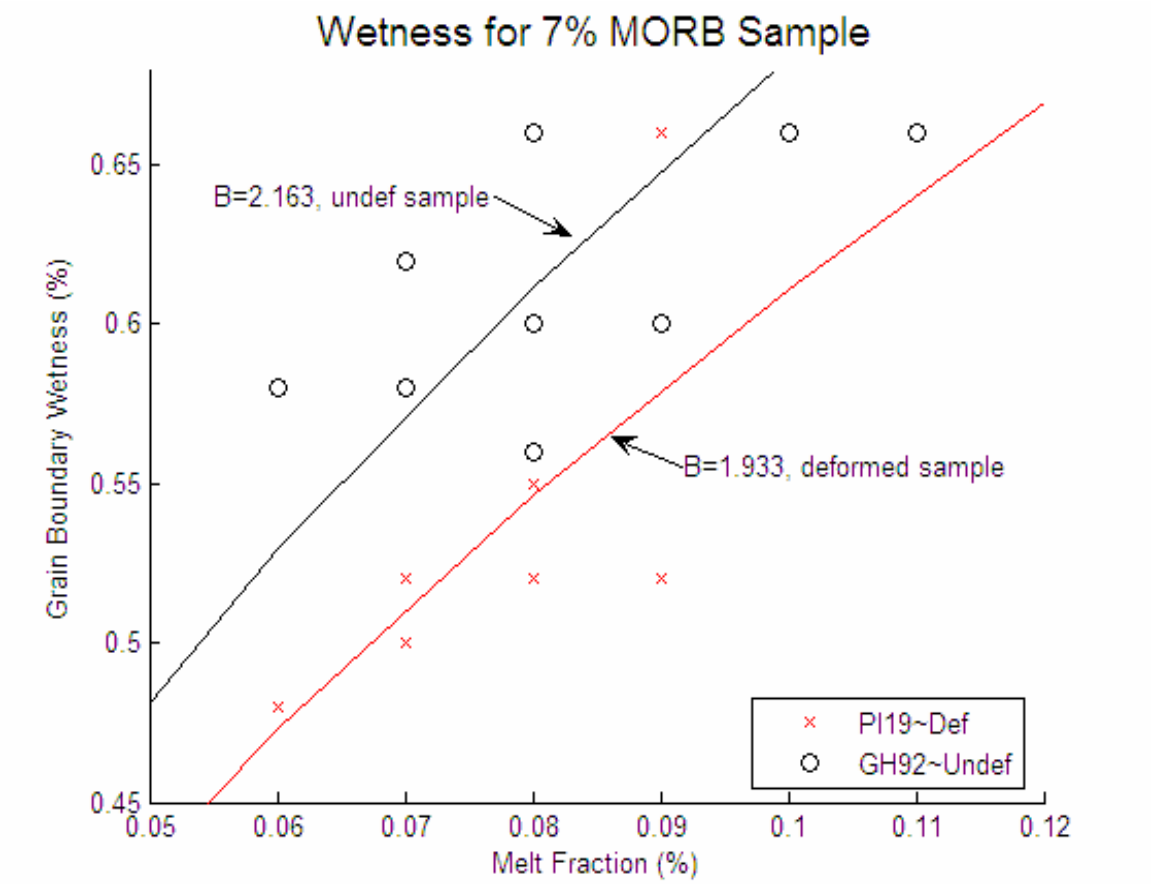

Figure 7. Wetness vs. melt fraction for the 7% MORB samples. The curves are fits of Eqn. 2, B values of 2.163 for the undeformed sample of 1241 and 1.933 for the deformed sample of 1241.

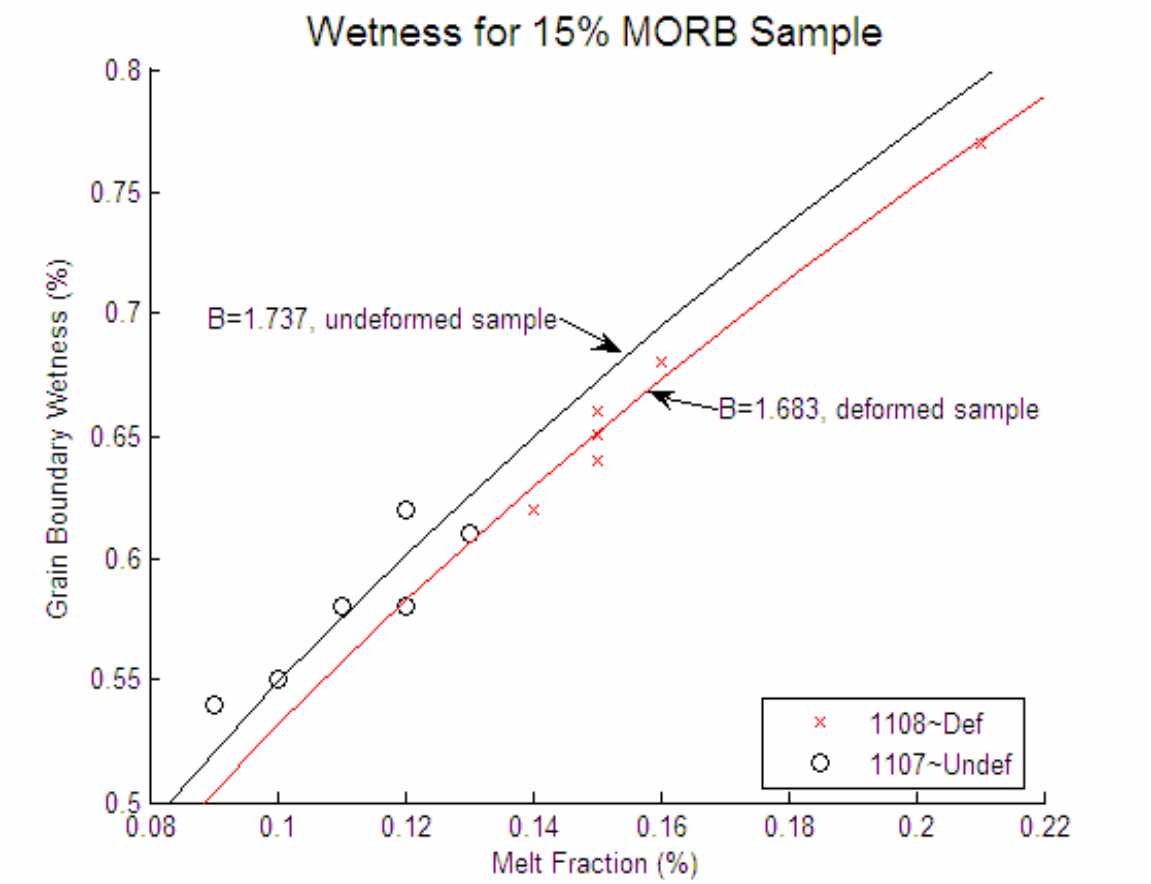

Figure 8. Wetness vs. melt fraction for the 15% MORB samples. The curves are fits of Eqn. 2, B values of 1.737 for the undeformed sample of 1241 and 1.683 for the deformed sample of 1241.

Figures 9 and 10 show the variation of A_{ss} and A_{sl} with melt fraction. The measurements are not inconsistent with the expectation that as melt fraction increases, A_{ss} should decrease and A_{sl} should increase. This is expected since an increasing amount of melt should place more melt-solid contacts at the expense of solid-solid contact. However, there is a lot of scatter in the measured contact areas, even at the same melt fraction. This scatter must arise from variations in the size and shape of both grains and pores between images. The role of grain size is indicated by the strong positive correlation between A_{ss} and A_{sl} shown in Figure 11: if the distribution and shape of the melts were similar in all images, and the grain and pore size varied together, this would produce a positive correlation A_{ss} and A_{sl} like the one observed. The total grain boundary area/unit area ($A_{ss} + A_{sl}$) for a given sample may vary between images by as much as a factor of 4. Taken together, these observations indicate a large variation in grain size between images.

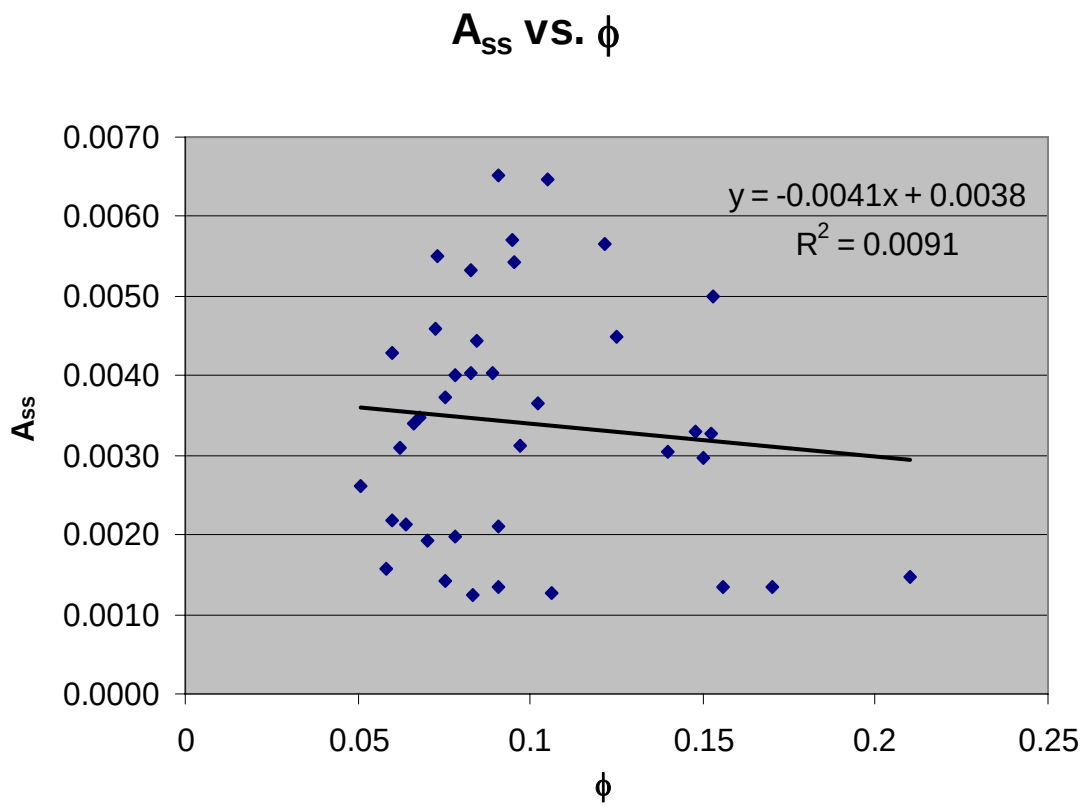

Figure 9. The area of the solid-solid grain contact vs. melt fraction for all images, and a linear fit to this data. A_{ss} should decrease with melt fraction, but the large variability for a given melt fraction is a function of changes in grain and pore size and shape.

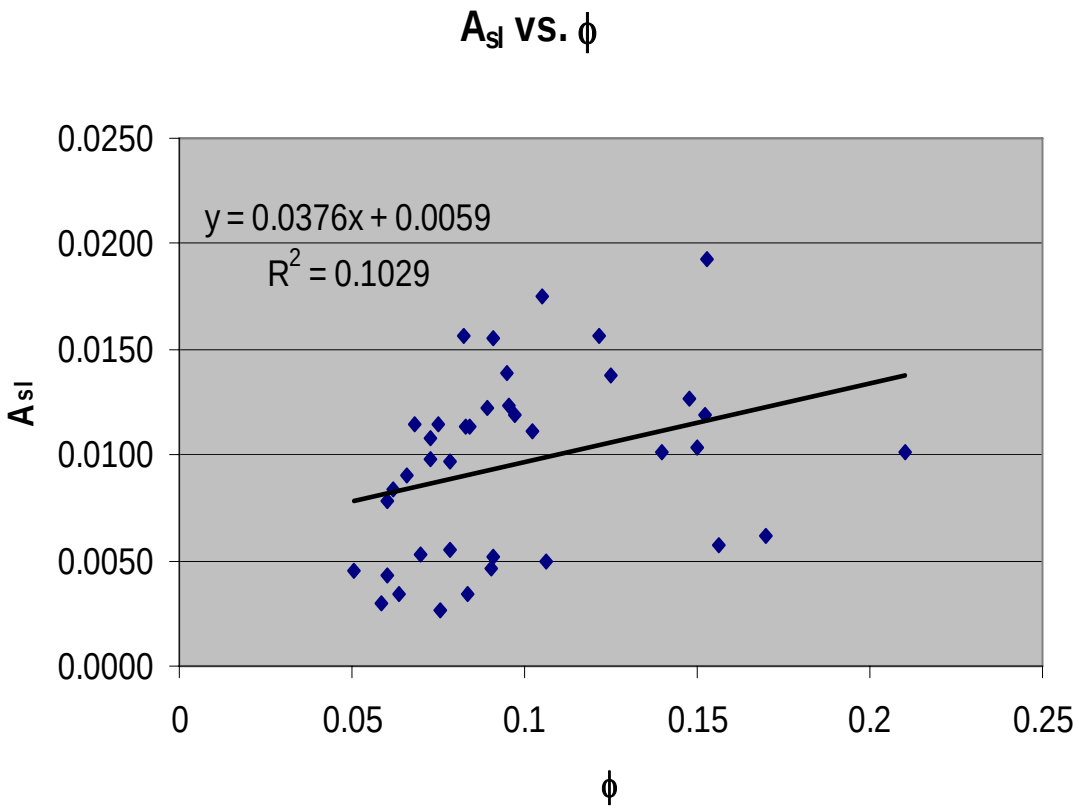

Figure 10. The area of the solid-liquid grain boundaries vs. melt fraction. As A_{sl} increases the melt fraction should increase.

Figure 12 has the same data as Figure 11, but it shows A_{sl} vs. A_{ss} with symbolized constituent melt fraction pairs. While all images of a particular sample show a similar linear trend, the data for the deformed and undeformed versions of a particular sample are distinct. This is partly due to systematic differences in melt fraction. For example in the 15% MORB samples, the images of the deformed sample have consistently higher melt fraction, and therefore larger A_{sl}. However these trends may also be partly due to changes in melt distribution. The 7% MORB samples have roughly the same range of melt fractions, but show a clearly different trend in A_{sl} in Figure 12.

Results of the measurements of grain boundary wetness ψ and melt fraction ϕ indicate that deformation does not have a consistent discernible effect on ψ. Each deformed and non-deformed sample set show different trends when comparing ψ vs. ϕ. Sample sets PI_19 and GH_92 show that ψ decreases with deformation. On the other hand, sample sets 1241 deformed and 1241 undeformed show that there is a slight effect, if any. Though, this could be due to a much lower melt fraction which caused some difficulty with image acquisition and processing. Finally, sample sets 1108 and 1107 show that ψ decreases with deformation.

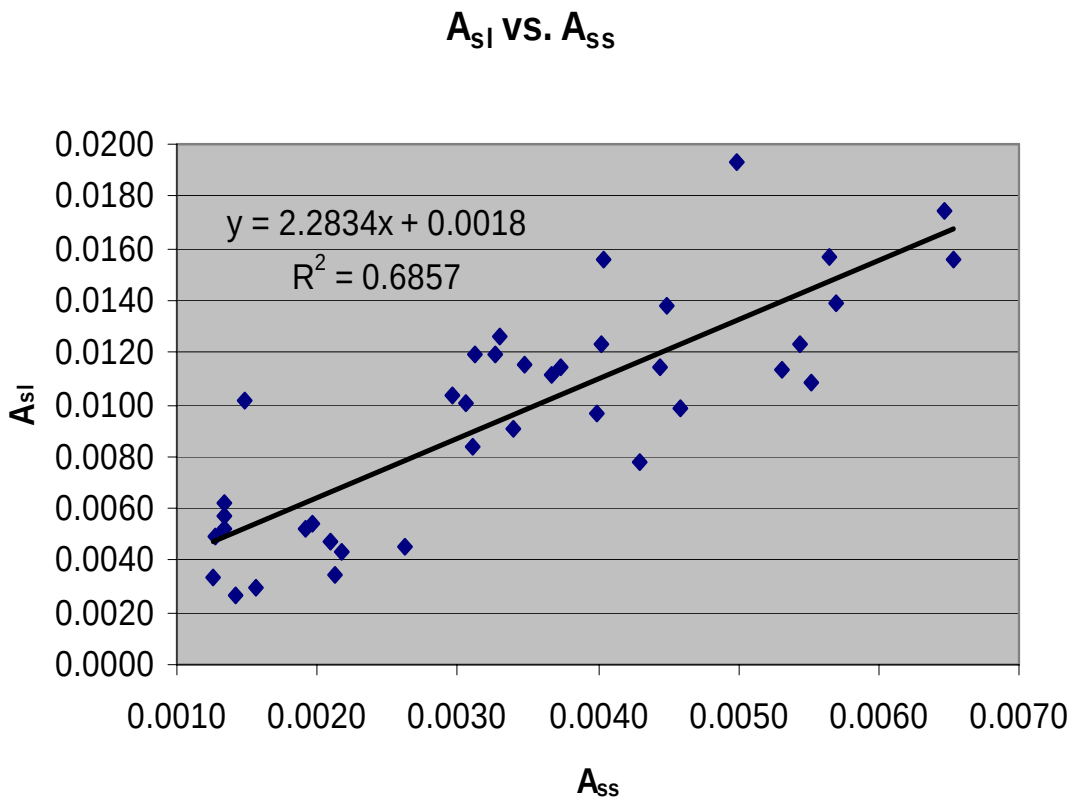

Figure 11. A_{sl} vs. A_{ss}, and the best fit line. There is a (+) direct relationship with A_{ss} and A_{sl}, as would be expected due to variations in grain size.

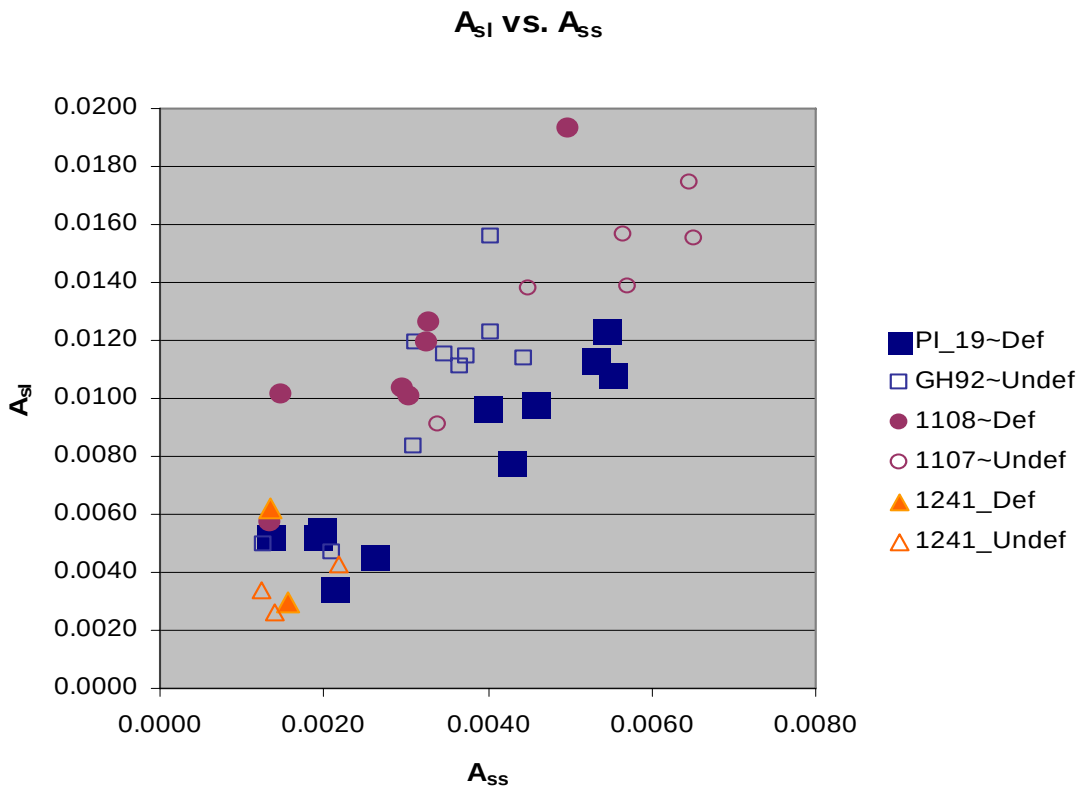

Figure 12. Same data shown in Figure 11., with different symbols used for the different samples. Although the images of each individual sample scatter along a linear trend due to grain size, the linear trends are not the same indicating real differences in grain boundary wetness.

4. DISCUSSION AND CONCLUSIONS

In this work, we developed an experimental and image analysis procedure that will be useful for future studies that measure wetness of partially molten peridotites. We found that in order to obtain the best SEM image for our purposes it is essential to polish the sample with .01 mm diamond lapping film and Syton for 4 minutes. This is invaluable information because the polish and topography of the sample is pertinent in imaging the samples. A bad quality image will not yield results. Lastly, we found that an effective way to calculate grain boundary wetness is to image the sample with a SEM, threshold it with Photoshop, and process it in Matlab.

Figure 5 and Table 1 show that effect of deformation on grain boundary wetness is not consistent among all samples. Deformation appears to significantly increase wetness in the intermediate melt fraction sample, very slightly increase wetness in higher melt fraction sample, and has little discernible effect in the low melt fraction sample. This observation is not consistent with Takei's [private communication, 2004] study of an organic analogue material, which found that grain boundary wetness was higher in deformed samples, compared to undeformed samples.

This disagreement between the analog and olivine/basalt systems could be due to a number of effects. The dependence of the interfacial energies on stress could be intrinsically different in the two systems. The magnitude of differential stress may also be important, since the analog experiments were conducted at much higher stresses.

Another possible reason for the disagreement could be some systematic error in the analysis. Each image was created through as close to the same procedure as possible, including a single method of polishing and preparing samples and processing images. The image analysis for each sample was repeated to ensure the reproducibility of the results. However, imaging very small amounts of melt is very difficult. Images with small melt fractions were not usable. So it's possible that the analytic method is missing small fractions of melt.

To better determine the effect of deformation on wetness, future studies might be done to observe the effect of deformation on partially molten peridotite at higher differential stresses. It might also be beneficial to keep track of total strain to assess that the amount of deformation is the same. With advances to technology, the SEM's may have higher resolutions and better all-around image quality. These advances in image quality would yield a more accurate representation of the olivine-basalt system thereby giving a more accurate calculation of grain boundary wetness.

REFERENCES

Bai, Q., Z-M., Jin, and H. W., Green, Experimental investigation of the rheology of partially molten peridotite at upper mantle pressures and temperatures, *Deformation enhanced Fluid Transport in the Earth's Crust and Mantle* (edited by Holness M. B.), Chapman and Hall, 40-61, 1997.

Bulau, J.R., H.S. Waff and J.A. Tyburczy, Mechanical and thermodynamic constraints on fluid distribution in partial melts, *J. Geophys. Res.*, 84, 6102-6108, 1979.

Cooper, R F., and D. L. Kohlstedt, Rheology and structure of olivine-basalt partial melts, *J. Geophys. Res*., 91, 9315-9323,1986.

Daines M.J. and Kohlstedt D.L., Influence of deformation on melt topology in peridotites, *J. Geophys. Res,*. 102, 10,257-10,271, 1997.

Daines M.J. and Kohlstedt D.L., A laboratory study of melt migration, *Phil. Trans. R. Soc. Lond* A, 342, 43-52, 1993

Hirth Greg and Kohlstedt D.L., Experimental constraints on the dynamics of the partially molten upper mantle: Deformation in the diffusion creep regime, *J. Geophys. Res.*, 100, 1981-2001, 1995.

Jin, z. M., H.W. Green, and Y. Zhou, Melt topology in partially molten mantle peridotite during ductile deformation, *Nature*, 372, 164 -167, 1994.

Riley, G.N. Jr., and D.L. Kohlstedt, Kinetics of melt migration in upper mantle-type rocks, *Earth Planet. Sci. Lett., 105*, 500-521, 1991.

Takei, Y., Constitutive mechanical relations of solid-liquid composites in terms of grain boundary-contiguity, *J. Geophys. Res., 103,* 18,183-18,203, 1998.

Takei, Y., Effect of pore geometry on VpNs: from equilibrium geometry to crack, *J. Geophys. Res., 1O7(B2),* 2050, doi:1O.1029/ 200lJBOO0522, 2002.

Takei, Y., Deformation-induced grain boundary wetting and its effects on the acoustic and rheological properties of partially molten rock analogue, *Submitted to J. Geophys. Res.*, 2005.

von Bargen, N., and H. S. Waff., Permeabilities, interfacial areas and curvatures of partially molten systems: Results of numerical computations of

equilibrium microstructures, *J. Geophys. Res.*, 91, 9261-9276, 1986.

Waff, H. S., and U. Faul., Effects of crystalline anisotropy on fluid distribution in ultramafic melts, *J. Geophys. Res*., 97, 9003-9014, 1992.

Watson, E. B., and J. M. Brenan., Fluids in the lithosphere, 1. Experimentally -determined wetting characteristics of CO2-H2O fluids and their implications for fluid transport, host-rock physical properties, and fluid inclusion formation, *Earth Planet. Sci. Lett.*, 85,497-515, 1987.

Yoshino Takashi, Takei Yasuko, Wark David A.,Watson E. Bruce., Grain boundary wetness of texturally equilibrated rocks, with implications for seismic properties of the upper mantle. Submitted to *J. Geophys*. *Res.*, 1-38, 2005

CONTACT INFORMATION

Name:	Stephen Edward Schneider
Address:	Department of Geology and Geophysics Texas A&M University College Station, TX 77840
Email Address:	sevrep@neo.tamu.edu
Education:	B.S., Geophysics, Texas A&M University, 2006